Physics in Medicine and Biology **56**, 105-115 (2011)

Use of contrast agents with fast field-cycling magnetic resonance imaging

Dara Ó Hógáin[1], Gareth R Davies[1], Simona Baroni[2], Silvio Aime[2,3] and David J Lurie[1]

[1]Aberdeen Biomedical Imaging Centre, University of Aberdeen, Foresterhill, Aberdeen AB25 2ZD, UK

[2]Invento S.r.l., Via Nizza 52, I-10126, Torino, Italy

[3]Department of Chemistry 'IFM', University of Torino, Italy

E-mail: d.lurie@abdn.ac.uk

Abstract

Fast Field-Cycling (FFC) MRI allows switching of the magnetic field during an imaging scan. FFC-MRI takes advantage of the T_1 dispersion properties of contrast agents to improve contrast, thus enabling more sensitive detection of the agent. A new contrast agent designed specifically for use with FFC was imaged using both a homebuilt FFC-MRI system and a 3 T Philips clinical MRI scanner. T_1 dispersion curves were obtained using a commercial relaxometer which showed large changes in relaxation rate between fields. A model of magnetization behaviour was used to predict optimum evolution times for maximum T_1 contrast between samples at each field. Images were processed and analysed to create maps of R_1 values using a set of images at each field. The R_1 maps produced at two different fields were then subtracted from each other in order to create a map of ΔR_1 in which pixel values depend on the change in R_1 of the sample between the two fields. The dispersion properties of the agent resulted in higher contrast in a ΔR_1 image compared with a standard T_1-weighted image.

PACS 87.61.Qr

Physics in Medicine and Biology

Key Words: Fast Field-Cycling, Contrast Agents, Manganese liposomes, ΔR_1 imaging

1. Introduction

In contemporary MRI, high magnetic fields (usually above 1.5 T) are used to generate high signal-to-noise ratio (SNR) (Redpath 1998). However, the T_1 values of different tissue types often tend to converge at higher field strengths (above 1.5 T), resulting in inherently lower T_1 contrast (Rinck *et al* 1988). While contrast agents can be used to improve the contrast between normal and pathological tissue, the relaxivity of the contrast agent is also dependent on magnetic field strength and tends to be lower at higher field strengths (Rinck *et al* 1988, Carlson *et al* 1992, Young *et al* 1981, Bloembergen 1957, Lauffer 1987). Clinical MRI scanners maintain a constant magnetic field B_0, so that image contrast is inevitably restricted to that which results from differences in tissue NMR parameters (especially T_1) at the scanner's fixed field. On the other hand, Fast Field-Cycling MRI (FFC-MRI) allows the field to be switched between two or more values in a time less than the T_1 of the sample, always returning to the same magnetic field for signal detection (Carlson *et al* 1992, Lurie *et al* 1998, Lurie *et al* 2010). Thus images can be produced at the magnetic field strength that optimizes contrast enhancement from contrast agents (Rinck *et al* 1988, Carlson *et al* 1992). This is done by analysing the dispersion curves of contrast agents and determining the field at which relaxivity (r_1) is highest. Furthermore, FFC-MRI allows access to a new type of contrast known as ΔR_1 contrast, in which signal intensity is based on the change in R_1 of a sample between different magnetic fields (Alford *et al* 2009).

This work examines the potential of a new contrast agent, designed for molecular imaging applications using FFC-MRI. Molecular imaging investigations usually require probes that can be detected at concentrations in the nano- or even pico-molar range. The agent used here takes the form of a liposome encapsulating Mn[II] ions in its inner aqueous cavity. Liposomes containing a large amount of paramagnetic Mn[II] ions are expected to display the high relaxation enhancement necessary to tackle the sensitivity issues present in MR molecular imaging assays (Aime *et al* 2009). The advantage of this contrast agent is the large change in its r_1 value from a high value at low fields (below 5 mT) to low r_1 at higher fields (above 60 mT), resulting in a large signal value in a ΔR_1 image. A comparison is made between ΔR_1 mapping using FFC-MRI and other imaging methods, including T_1-weighted imaging and T_1 mapping at 3 mT, 59 mT and at a standard clinical field of 3 T. Contrast is seen to improve using ΔR_1 mapping. Moreover it is expected that such a system may show both good specificity and *in vivo* tolerability, as liposomes are commonly used as drug delivery agents to target diseased tissue and living organisms should be able to control the small excess of essential Mn[II] ions.

In order to demonstrate proof of purpose of this novel technique, it was considered sufficient to carry out experiments *in vitro*. The results show how contrast agent conspicuity can be improved using FFC-MRI. Future studies are planned which will show *in vivo* validation of this new technique at carefully selected magnetic fields.

2. Magnetization Behaviour during field cycling

The contrast in a T_1-weighted inversion-recovery image is largely dependent on the inversion time (*TI*) used. To optimize the contrast between two samples it is important to understand how the magnetization behaves with inversion time during a pulse. For a fixed-field inversion-recovery pulse sequence the magnetization behaviour can be described by the equation below.

$$M(TI) = M_0\left(1 - 2\exp\left(\frac{-TI}{T_1}\right)\right) \quad (1)$$

Where *M(TI)* is the magnetization at a time (*TI*) after the inversion pulse, M_0 is the equilibrium magnetization at the readout field, and T_1 is the longitudinal relaxation time constant of the sample. The optimum inversion time for maximum contrast between two samples with T_1 values T_{1a} and T_{1b} can be determined using the equation below (Ahrens et al 1998).

$$TI_{opt} = \frac{T_{1a}.T_{1b}}{(T_{1b} - T_{1a})}\ln\left(\frac{T_{1b}}{T_{1a}}\right) \quad (2)$$

However magnetization behaves differently during field-cycling, as the T_1 value changes between one field and another, thus magnetization evolves at different rates at each field as shown in figure 1.

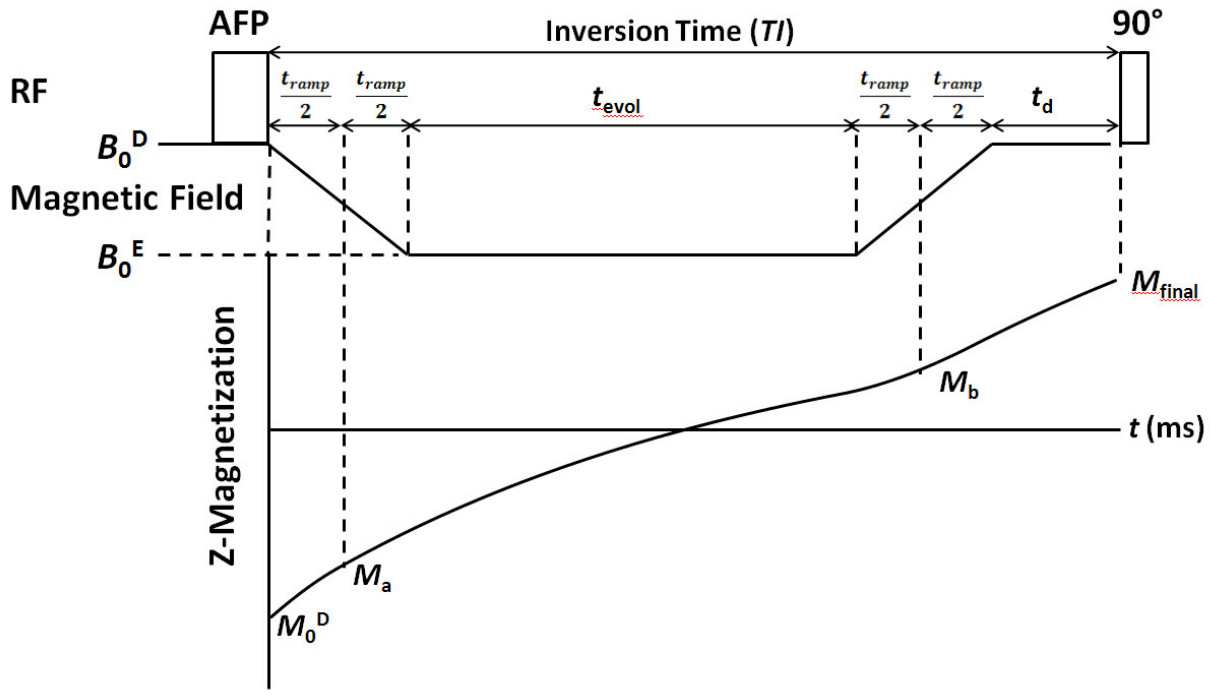

Figure 1: Field-cycling inversion recovery pulse sequence, and magnetization curve, with magnetization values identified at four points M_0^D, M_a, M_b and M_{final}.

Following inversion by adiabatic fast passage (AFP) the magnetic field is ramped rapidly (in a time $t_{ramp} \approx 40ms$) from the readout field (B_0^D), to a selected evolution field (B_0^E). The sample's T_1 value at these fields is designated as T_1^D and T_1^E respectively.

The magnetization of the sample is allowed to evolve at the evolution field for a time period (t_{evol}). The system then ramps back up to the acquisition field followed by a delay time (t_d) in order for the magnet to stabilize before a 90° pulse is applied. This is then followed by a gradient echo imaging sequence. The magnetization evolves continuously during the ramp time t_{ramp} , the evolution time t_{evol} and the delay time t_d. As the ramp time is short relative to the evolution time, the ramp between the two fields can be considered as a step process with half of the time spent at the higher field, and half the time at the lower field. The magnetization can be split into four separate stages during the pulse sequence; M_0^D, M_a, M_b and M_{final} as shown in figure 1. M_a is given by

$$M_a = M_0^D\left(1-2\exp\left(-\frac{\left(t_{ramp}/2\right)}{T_1^D}\right)\right) \tag{3}$$

where M_0^D is the equilibrium magnetization at the readout field. M_b is described by

$$M_b = M_0^E - \left(M_0^E - M_a\right)\exp\left(-\frac{\left(t_{evol}+t_{ramp}\right)}{T_1^E}\right) \tag{4}$$

In this case M_0^E is the equilibrium magnetization at the evolution field obtained using the ratio, $B_0^D/B_0^E = M_0^D/M_0^E$. M_{final} is the final magnetization described by

$$M_{final} = M_0^D + \left(M_b - M_0^D\right)\exp\left(-\frac{\left(t_d + t_{ramp}/2\right)}{T_1^D}\right) \tag{5}$$

Substituting M_a and M_b into M_{final} gives a full description of the magnetization behaviour during an FFC inversion recovery pulse sequence.

$$M_{final} = M_0^D + \left\{M_0^E - M_0^D - \left\{M_0^E - M_0^D + 2M_0^D\exp\left[-\frac{\left(t_{ramp}/2\right)}{T_1^D}\right]\right\}\exp\left[-\frac{\left(t_{evol}+t_{ramp}\right)}{T_1^E}\right]\right\}\exp\left[-\frac{\left(t_d+t_{ramp}/2\right)}{T_1^D}\right] \tag{6}$$

This equation was used to predict magnetization behaviour for a number of different samples with a range of T_1 time constants at different fields. To validate the equation a comparison was made with experimental data. Using this equation it was possible to select the evolution times which would give maximum contrast between any two samples using T_1-weighted imaging techniques at different field strengths.

3. Methods

3.1. Sample Preparation

All the phospholipids used in the liposome preparation were purchased from Avanti Polar; $MnCl_2$ was purchased from Sigma Aldrich. Mn(II)-loaded liposomes were prepared by using a mixture of phospholipids (POPC = 1-palmitoyl-2-oleoyl-sn-glycero-3-phosphocholine, 95% and DSPE-PEG_{2000} =

1,2-distearoyl-sn-glycero-3-phospoethanolamine-N-[metoxy(polyethylene glycol)-2000), 5%). The thin lipidic method was followed (Lasch *et al* 2003). Briefly, the lipids (about 30 mg/ml) were dissolved in chloroform and the organic solution was slowly evaporated for removing the solvent until a thin film was formed. The film was then hydrated at 55 °C with a 5 mM aqueous solution of $MnCl_2$, whose osmolarity was corrected to 300 mOSm with NaCl. The resulting suspension of multilamellar vesicles (MLV) was extruded (Lipex extruder, Northern Lipids Inc., Canada) through progressively smaller pore sizes (polycarbonate filters with pore diameters of 400, 200 and 100 nm, respectively). The final suspension of liposomes was purified from the not encapsulated metal ions by exhaustive dialysis against a HEPES (N-2-hydroxyethylpiperazine-N'-2-ethanesulfonic acid)/NaCl buffer (pH 7.4, 300 mOsm). The liposomes were characterized by dynamic light scattering (Zetasizer NanoZS, Malvern, UK) in order to assess the mean hydrodynamic size and the polydispersity of the system. The liposomes used in this work showed an average diameter of 111 nm; the polydispersity index (PDI) was smaller than 0.1. Mn[II] concentration in the liposome suspension was determined by T_1 measurement after the disruption of the liposomes' membranes by mineralization with HCl. A stock liposome suspension corresponding to a total Mn[II] concentration of 0.77 mM was used for the preparation of an imaging phantom.

The suspension was diluted in HEPES/NaCl buffer solution in order to prepare three samples at the following concentrations: A: 0.8mM, B: 0.045 mM, C: 0.035 mM. A solution of 0.23 mM Prohance was also prepared in de-ionized water in order to provide comparison with the Mn[II] contrast agent. Prohance is a standard contrast agent comonly used in clinical MRI scans but unlike Mn[II] shows very little change in R_1 between field strengths.

3.2. Dispersion Curve Measurement

The samples were placed in NMR tubes and dispersion curves were measured. The dispersion curve shape of each sample depends on a combination of factors including; the concentration of the agent in the solution, the concentration of the entrapped paramagnetic molecule within the liposome, the type of paramagnetic species, the viscosity of the hydration solution, which gives rise to a peak at high fields, the membrane composition which affects the water exchange time, and the total size of the liposome, which relates to the reorientational correlation time.

Dispersion curves were obtained experimentally using a field-cycling pulse sequence on a commercial NMR relaxometer (Stelar S.r.l., Italy). Pre-polarization was typically at 187 mT, with detection at 169

mT. At each value of the evolution field the sequence was repeated using N different values of the inversion time (*TI*), allowing T_1 to be calculated as a function of magnetic field (Ferrante and Sykora 2004).

3.3. Imaging

An imaging phantom was constructed containing samples of Mn[II] contrast agent solutions arranged alongside a 0.23 mM sample of Prohance. The samples were contained in glass tubes with dimensions 1 cm diameter x 2 cm length. Samples were imaged on both a homebuilt whole-body FFC-MRI system (Lurie *et al* 1998), and a 3 T Philips Achieva clinical MRI scanner. The FFC-MRI system employed two coaxial magnets. The primary permanent magnet provides a homogeneous fixed detection field of 58.7 mT (2.5 MHz proton frequency), while the secondary resistive electromagnet provided a variable offset field, capable of ramping from 0 to 58.7 mT in 40 ms (Lurie *et al* 1998). During the ramp time the magnetic field changes linearly with time until the desired evolution field strength is reached. Following the ramp time there is a brief period of slight magnetic field instability (< 1 mT) caused by the time it takes the amplifier to switch off completely as well as by eddy currents induced in the coil. This instability occurs over a short time period and has negligible effect on the final bulk magnetization as described by equation 6. However a short delay has been implemented following field cycling ramps and before any RF pulse are applied, so that this instability does not affect the RF pulse efficiency. The total homogeneity of the evolution field was within 500 ppm. The stability of the evolution field is dependant on the current supply to the electromagnet, and has been found to vary by up to 1% which is stable enough not to affect the T_1 value of the sample.

3.3.1. T_1 weighted imaging. T_1 weighted images were acquired using the FFC-MRI scanner at 59 mT and 3 mT using a range of evolution times at each field, with evolution times carefully selected to show the maximum contrast between each Mn[II] sample and the Prohance sample. The inversion time following an inversion pulse is equivalent to the evolution time plus an additional 150 ms (which includes the time needed for both the ramp times (each 40 ms duration) plus the delay time (70 ms) before the 90° pulse. The fields were selected to show maximum change in R_1 of the Mn[II] contrast agent. An FFC inversion recovery imaging pulse sequence was used as shown in figure 1, but with the addition of imaging

gradients and a selective 90° pulse. The matrix size was 64 x 64, with number of excitations (NEX) = 1. Image slice thickness was 0.8 cm, and the field of view (FOV) was 8 cm.

T_1-weighted images were also acquired at 3 T using a Philips clinical MRI scanner, with a slice thickness of 0.8 cm and an FOV of 6 cm. The imaging phantom was placed in a knee coil and images were produced using a standard spin-echo inversion-recovery pulse sequence with a range of inversion times. The samples' T_1 times were much longer at 3 T compared with 59 mT, thus a much wider range of inversion times was selected to produce an accurate R_1 map.

3.3.2. ΔR_1 mapping. A disadvantage of T_1-weighted imaging in FFC-MRI is that the signal is dependent not only on the T_1 value of the sample but also on the equilibrium magnetization at the evolution field (M_e) (Ungersma *et al* 2006, Alford *et al* 2009). The intensity values shown in a ΔR_1 map however depend solely on the change in R_1 between fields and can take full advantage of the dispersion characteristics of the contrast agent. ΔR_1 mapping is a similar technique to T_1 mapping which is used in MRI to allow quantitative analysis of the distribution of contrast agents *in vivo* (Treier *et al* 2008). This technique first processes a series of images taken at multiple evolution times, and creates a map of R_1 values for each pixel. R_1 maps created at different fields can then be subtracted from each other to create a map of ΔR_1 values, representing the change in R_1 of the samples between the two fields.

4. Results

4.1. Dispersion Curve Measurement

Figure 2 shows the measured dispersion curve of the 0.77 mM Mn[II] sample.

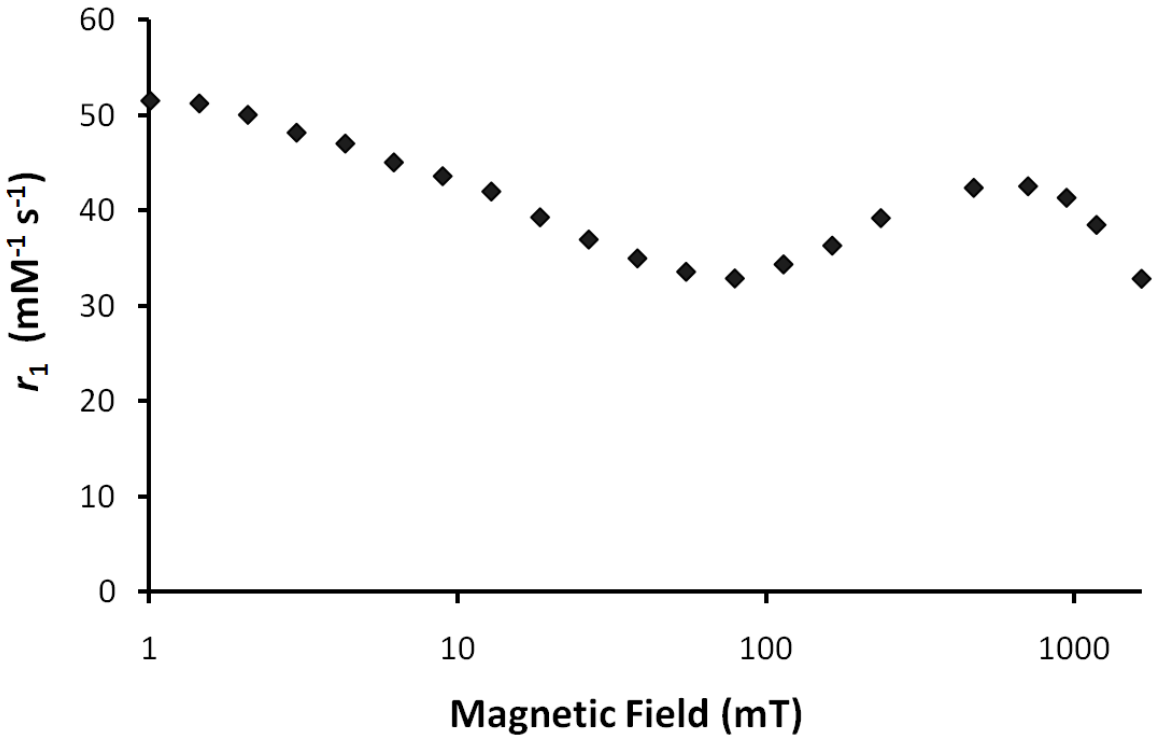

Figure 2: T_1 dispersion curve of 0.77 mM Mn[II] liposome samples at 25°C. Measured using a Stelar SPINMASTER relaxometer.

The 0.77 mM stock solution was diluted in a HEPES buffer solution and dispersion curves were acquired at different final concentrations of Mn[II] as shown in figure 3; a dispersion curve of 0.23 mM Prohance solution is also shown.

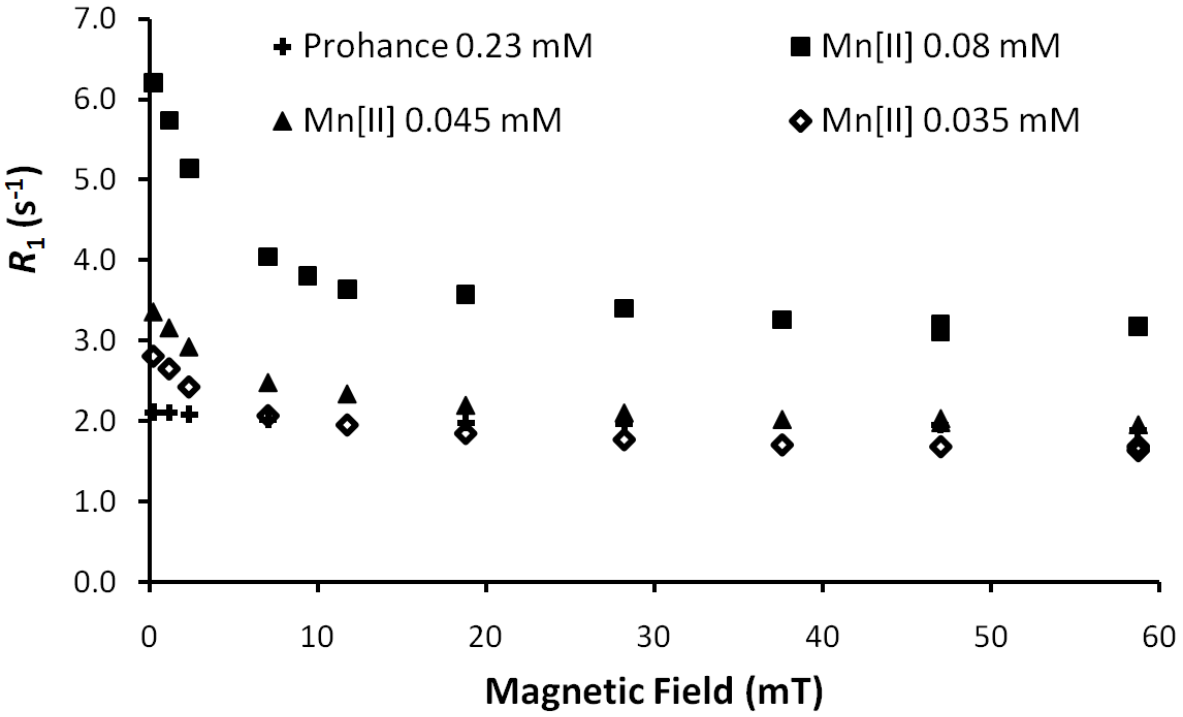

Figure 3: T_1 dispersion curves of Mn[II] Liposomes and Prohance sample at 25°C. Measured using a Stelar SMARtracer relaxometer.

The sample with the highest concentration of Mn[II] shows a change of ~ 3 s^{-1} between 3 mT and 59 mT, whereas the 0.23 mM Prohance sample only shows a change of ~ 0.2 s^{-1} over the same field range. Thus the difference between these samples should be clearly distinguishable in a ΔR_1 map.

4.2. T_1 weighted imaging

An imaging phantom containing samples of Mn[II] liposomes and a sample of Prohance was imaged at 59 mT with an inversion time of 750 ms as shown in figure 4 (a). The imaging phantom was then imaged at a range of inversion times at both 59 mT and 3 mT as shown in figure 4 (b) and (c) respectively, and finally at 3 T using a Philips clinical MRI scanner as shown in figure 4 (d).

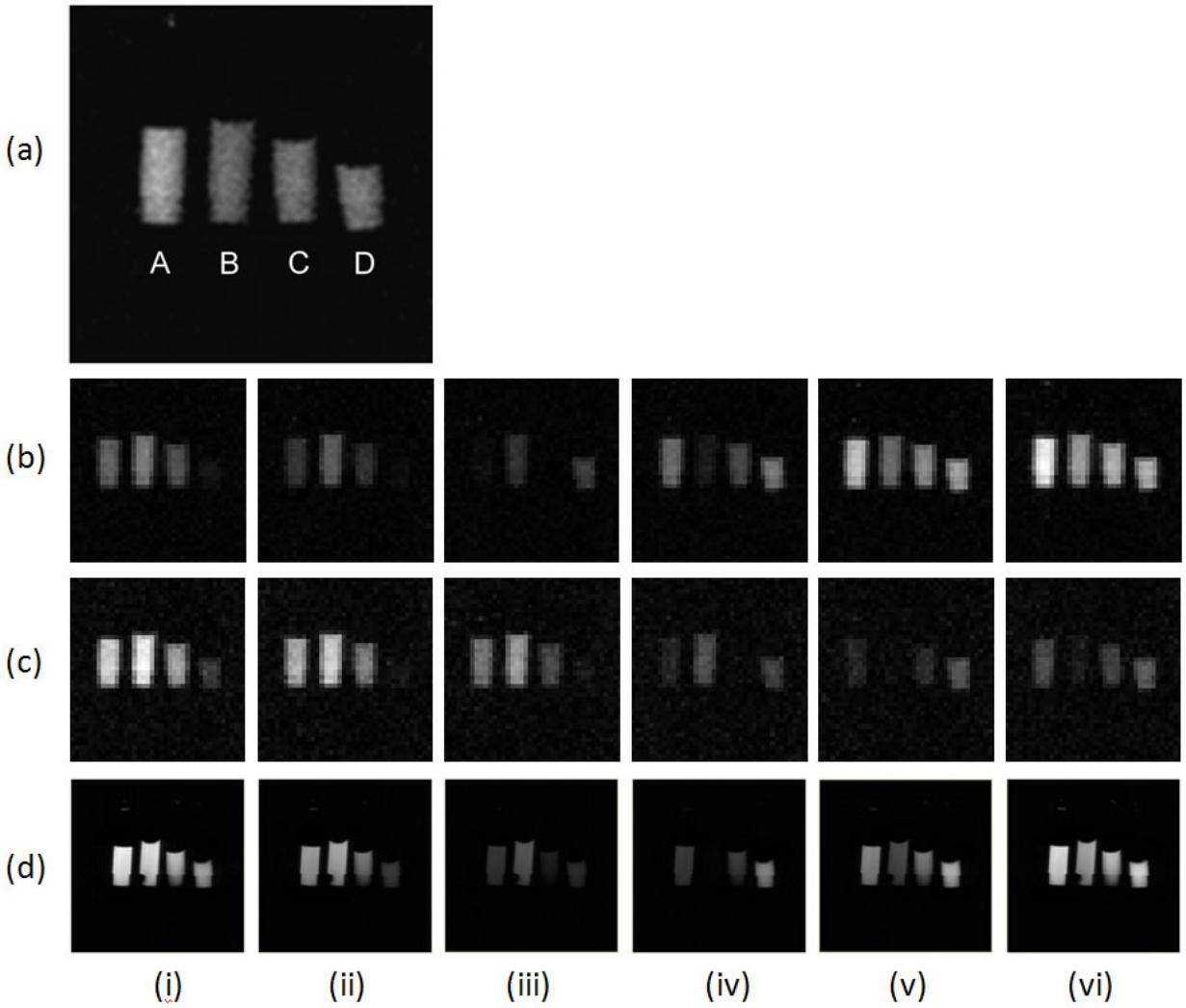

Figure 4: Phantom image, obtained using an FFC inversion recovery pulse sequence (a) at 59 mT with inversion time of 750 ms A: Prohance 0.23 mM, B: Mn[II] 0.08 mM, C: Mn[II] 0.05 mM, D: Mn[II] 0.03 mM. (b) 59 mT at a range of inversion times: (i) 190 ms (ii) 240 ms (iii) 370 ms (iv) 590 ms (v) 850 ms (vi) 1150. (c) 3 mT at a range of evolution times: (i) 190 ms (ii) 240 ms (iii) 370 ms (iv) 590 ms (v) 850 ms (vi) 1150 ms. Imaging parameters are as follows: matrix size = 64 x 64, NEX = 1, Repetition time = 1.5 s, Field of view = 8 cm, slice thickness = 0.8 cm. Total imaging time was 63 minutes. (d) 3 T at a range of inversion times (i) 50 ms (ii) 200 ms (iii) 400 ms (iv) 700 ms (v) 950 ms (vi) 1600. Imaging parameters were as follows: slice thickness 0.8 cm, FOV 6 cm, total imaging time for all images was 20 minutes.

4.3. Magnetization Model

A region of interest was selected for each sample in all of the T_1 weighted images, and the mean signal and standard deviation were measured. The mean signal was then plotted against evolution time. This experimental data was then compared with predicted magnetization curves (figure 5) obtained using equation 6. For clarity, only curves from two samples are shown corresponding to (a) Mn[II] 0.8 mM with T_1 of 181 ms at 3 mT and (b) Prohance 0.23 mM with T_1 of 471 ms at 3 mT. Values for T_1^0 and T_1^e used in equation 6 were obtained from relaxometry data, and M_e was calculated using the ratio $B_0/B_e = M_0/M_e$.

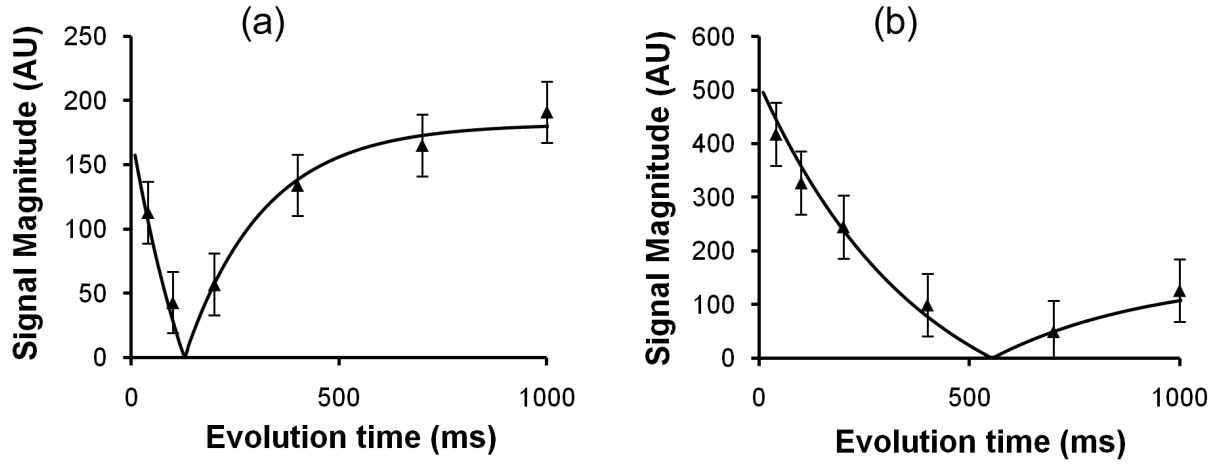

Figure 5: A comparison between experimental (triangle) and predicted (solid line) signal magnititude vs. evolution time at 3 mT for (a) 0.08 mM Mn[II] sample, and (b) 0.23 mM Prohance sample.

The experimental data was seen to match the predicted magnetization curve within experimental error, thus demonstrating that equation 6 could be used to predict magnetization behaviour during a field-cycling inversion-recovery pulse sequence. The model could therefore be used to predict contrast as a function of evolution time in order to optimize T_1-weighted contrast at any evolution field value.

4.4. ΔR_1 Mapping

A ΔR_1 map was produced by first creating maps of R_1 values at 59 mT and 3 mT. The R_1 maps were constructed using a program written in MATLAB (MathWorks, Natick, MA, USA) which overlaid a set of T_1-weighted images acquired at a range of evolution times using an inversion-recovery pulse sequence. The MATLAB program plotted signal intensity against evolution time to determine the R_1 value for each pixel in the set of images. R_1 maps were then subtracted to give a map of ΔR_1.

R_1 maps obtained at 59 mT and 3 mT are shown in figures 6a and 6b, and a map of ΔR_1 values is shown in figure 6c. In the R_1 maps the contrast between the Mn[II] samples and the Prohance sample increases when the field is switched to 3 mT due to the diverging relaxation rates at low field. The ΔR_1 map however shows higher contrast between the Mn[II] samples and the Prohance sample than either of the fixed-field R_1 maps.

The measurement of the R_1 value was found to have a standard deviation of ~10% and ~15% at 59 mT and 3 mT respectively, while the standard deviation for the ΔR_1 map is ~25%. Uncertainty is dependent on a number of factors including the inherent signal-to-noise ratio, the variation of the sample magnetization with field, the number of evolution times used, and the number of signal averages used for each image (Ferrante and Sykora 2004).

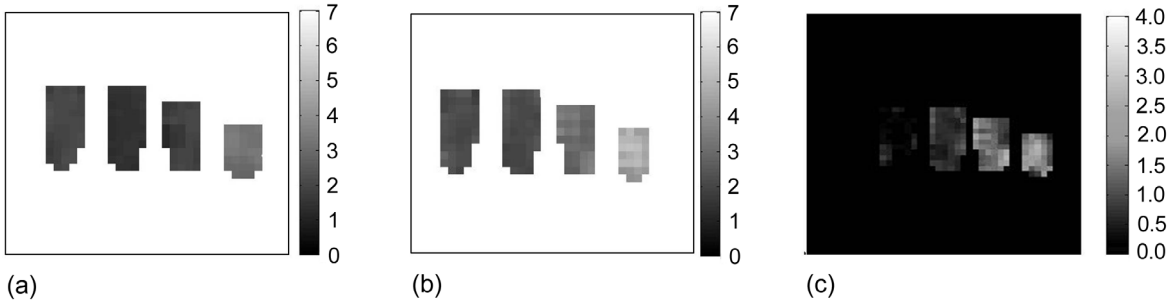

Figure 6: Sections from R_1 maps obtained at (a) 59 mT, (b) 3 mT; (c) ΔR_1 map obtained by subtracting R_1 maps shown in (a) and (b).

4.5. Image Analysis

The contrast between Mn[II] liposome and Prohance samples was compared using contrast-optimized T_1-weighted imaging at 3 T, 59 mT, 3 mT and ΔR_1 mapping. In order to compare contrast using these different imaging modalities the contrast between the Mn[II] samples and the Prohance sample was first defined as follows (Hendrick and Raff 1992):

$$\text{Contrast ratio (\%)} = \frac{(S_A - S_B)}{(S_A + S_B)} \times 100 \qquad (7)$$

As shown in figure 7, this comparison reveals that contrast is significantly increased using ΔR_1 mapping compared with T_1-weighted imaging. In particular, the contrast ratio between 1.0 mM Prohance and 0.045 mM Mn[II] samples (with T_1 values of 812 ms and 765 ms respectively) in the T_1-weighted image obtained at 3 T is 36%. The contrast between these samples increases to 78% using ΔR_1 imaging which shows how the Mn[II] agent can be detected with significantly greater sensitivity using ΔR_1 mapping. It should be noted that the enhanced contrast is observed using data obtained at 3 mT and 59 mT, i.e. between one fiftieth and one thousandth of the field used in the high-field experiment.

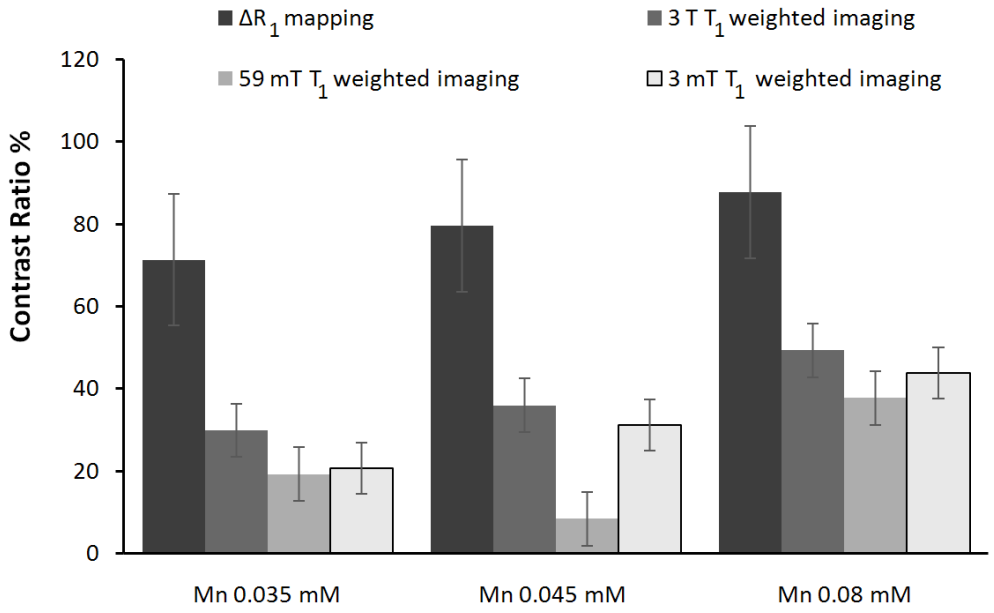

Figure 7: Comparison of contrast ratio from T_1-weighted images and ΔR_1 image. Error bars are based on standard deviation across the images.

5. Discussion

The contrast between different concentrations of a new Mn[II] liposome-based contrast agent and a conventional agent (Prohance) was compared using different imaging methods. These imaging methods included T_1-weighted imaging at 3 mT, 59 mT, and 3 T, and ΔR_1 mapping. Multiple images were used to produce a ΔR_1 map which allowed a quantitative analysis of the change in R_1 between different fields. This method suppressed the values from the Prohance sample, increased the sensitivity of detection of the Mn[II] agents, and showed that the ΔR_1 values were proportional to the concentration of the Mn[II] contrast agent. Furthermore the liposome sample used here of 111 nm diameter contains ca. 10^3 Mn[II] ions[1]. Thus suspensions containing 0.15 mM and 0.06 mM Mn[II] ions correspond to ca. 60 and 30 nM concentration of liposomes, respectively. The observed ΔR_1 enhancements clearly indicate that the proposed method (FFC-MRI and dispersion-tailored reporting probe) is well suited for molecular imaging applications. The present FFC-MRI system has shown consistency in its measurements and has provided proof-of-principle that ΔR_1 mapping can be used to improve the conspicuity of tailored contrast agents. However the error inherent in ΔR_1 mapping remains a significant problem as it reduces the sensitivity of the technique to detect small changes in R_1. In order to reduce error and improve sensitivity, more averages and more evolution times could be used in image acquisition. Unfortunately this would lead to longer imaging times. At present the time needed to produce multiple images at different field strengths is approximately 63 minutes, which is clearly too long for a clinical scan. However this time may be reduced using a faster T_1 mapping sequence such as an inversion-recovery Look-Locker echo-planar imaging sequence (Look and Locker 1970, Shin *et al* 2009).

The main challenge to applying ΔR_1 mapping *in vivo* is to know at which fields to image in order to optimize contrast enhancement in a ΔR_1 map. This information can be obtained by acquiring dispersion curves *in vivo* of tissue with and without the contrast agent. To this end further work has been carried out in parallel to this study, to obtain localized dispersion curves *in vivo*. (Pine *et al*, 2009). The relaxation curves of biological tissues have been studied extensively (Bottomley *et al* 1984, Escanye *et al* 1982, Fischer *et al* 1990) and tend to show relatively little change in R_1 at field strengths above 200 mT, whereas the Mn liposome samples exhibit large changes in R_1 within this field range (as shown in figure 2). To carry out *in vivo* experimental work a new FFC-MRI system with a field range between 0 and 0.5

[1] The determination of the number of Mn[II] per liposome has been assessed by measuring the absorbance of a fluorescent dye added to the hydration solution of Mn[II] ions (Zuidam et al 2003).

tesla has been built in our laboratory and is in its final testing stages. This system will have improved field homogeneity, faster ramp times and a higher detection field, allowing more accurate and improved ΔR_1 mapping using FFC.

Acknowledgements

The authors acknowledge financial support for the FFC-MRI project from Research Councils UK and the Engineering and Physical Sciences Research Council, under the Basic Technology scheme (grant no. EP/E036775/1). They thank Mr. Azlan Bin Che Ahmad for his assistance with the measurements at 3 T.

References

Ahrens E T, Rothbächer U, Jacobs R E and Fraser S E 1998 A model for MRI contrast enhancement using T_1 agents *Proc. Natl. Acad. Sci. USA* **95** 8443–8

Aime S, Delli Castelli D, Geninatti Crich S, Gianolio E and Terreno E 2009 Pushing the sensitivity envelope of lanthanide based magnetic resonance imaging (MRI) contrast agents for molecular imaging applications *Acc. Chem. Res.* **42** 822-831

Alford J K, Rutt B K, Scholl T J, Handler W B and Chronik B A 2009 Delta relaxation enhanced MR: improving activation-specificity of molecular probes through R_1 dispersion imaging *Magn. Reson. Med.* **61** 796–802

Bloembergen N 1957 Proton relaxation times in paramagnetic solutions *J. Chem. Phys.* **27** 572-573

Bottomley P A, Foster T H, Argersinger R E and Pfeifer L M 1984 A review of normal tissue hydrogen NMR relaxation times and relaxation mechanisms from 1-100 MHz *Med. Phys.* **11** 425

Carlson J W, Goldhaber D M, Brito A and Kaufman L 1992 MR relaxometry imaging. Work in progress *Radiology* **184** 635-639

Escanye J M, Canet D and Roberta J 1982 Frequency dependence of water proton longitudinal nuclear magnetic relaxation times in mouse tissues at 20°C *Biochim. Biophys. Acta.* **721**, 305-311

Ferrante G and Sykora S 2004 Technical aspects of fast field-cycling relaxometry *Adv. Inorg. Chem.* **57** 405-470

Fischer H W, Rinck P A, Van Haverbeke Y and Muller R N 1990 Nuclear relaxation of human brain gray and white matter: analysis of field dependence and implications for MRI *Magn. Reson. Med.* **16**, 317-34.

Hendrick R E and Raff U 1992 *Magnetic Resonance Imaging* (2nd ed.). St. Louis: Mosby. 109–144.

Lasch J, Weissig V and Brandl M 2003 Preparation of liposomes, in *Liposomes - A Practical Approach*, *2nd edition,* ed V P Torchilin and V Weissig (Oxford: Oxford University Press) p 3

Lauffer R B 1987 Paramagnetic metal complexes as water proton relaxation agents for NMR imaging: theory and design *Chem. Rev.* **87** 901-927

Look D C and Locker D R 1970 Time saving in measurement of NMR and EPR relaxation times. *Rev. Sci. Instrum.* **41** 250-251

Lurie D J, Foster M A, Yeung D and Hutchison J M S 1998 Design, construction and use of a large-sample field-cycled PEDRI imager *Phys. Med. Biol.* **43** 1877-1886

Lurie D J, Aime S, Baroni S, Booth N A, Broche L M, Choi C-H, Davies G R, Ismail S, Ó hÓgáin D and Pine K J 2010 Fast field-cycling magnetic resonance imaging *Comptes Rendus Physique* **11** 136-148

Pine K J, Davies G R and Lurie D J 2009. Field-cycling NMR relaxometry with spatial selection. *Magn. Reson. Med.,* **63** 1698-1702

Redpath T W 1998 Signal-to-noise ratio in MRI *Br. J. Radiol*. **71** 704-707

Rinck P A, Fischer H W, Vander Elst L, Van Haverbeke Y and Muller R N 1988 Field-cycling relaxometry: Medical applications *Radiology* **168** 843-849

Shin W, Gu H and Yang Y 2009 Fast high-resolution T_1 mapping using inversion recovery Look-Locker echo planar imaging at steady state: Optimization for accuracy and reliability *Magn. Reson. Med.* **61** 899-906

Treier R, Steingoetter A, Goetze O, Fox M, Fried M, Schwizer W and Boesiger P 2008 Fast and optimized T_1 mapping technique for the noninvasive quantification of gastric secretion *J. Magn. Reson. Imaging* **28** 96-102

Ungersma S E, Matter N I, Hardy J W, Venook R D, Macovski A, Conolly S M and Scott G C 2006 Magnetic resonance imaging with T1 dispersion contrast *Magn. Reson. Med.* **55**, 1362-1371

Young I R, Clarke G J, Bailes D R, Pennock J M, Doyle F H and Bydder G M 1981 Enhancement of relaxation rate with paramagnetic contrast agents in NMR imaging *J. Comput. Tomogr.* **5** 543-547

Zuidam N J, de Vrueh R and Crommelin D J A 2003 Characterization of liposomes, in *Liposomes - A Practical Approach* , *2nd edition,* ed V P Torchilin and V Weissig (Oxford: Oxford University Press) p 31